

# Probabilistic Radio-Visual Active Sensing for Search and Tracking

Luca Varotto<sup>1</sup>, Angelo Cenedese<sup>1</sup>, and Andrea Cavallaro<sup>2</sup>

**Abstract**—Active Search and Tracking for search and rescue missions or collaborative mobile robotics relies on the actuation of a sensing platform to detect and localize a target. In this paper we focus on visually detecting a radio-emitting target with an aerial robot equipped with a radio receiver and a camera. Visual-based tracking provides high accuracy, but the directionality of the sensing domain often requires long search times before detecting the target. Conversely, radio signals have larger coverage, but lower tracking accuracy. Thus, we design a Recursive Bayesian Estimation scheme that uses camera observations to refine radio measurements. To regulate the camera pose, we design an optimal controller whose cost function is built upon a probabilistic map. Theoretical results support the proposed algorithm, while numerical analyses show higher robustness and efficiency with respect to visual and radio-only baselines.

## I. INTRODUCTION

Active sensing consists of controlling the sensor state to gather (more) informative observations [1] or to accomplish a task (e.g., find a target within a certain time budget [2]). This control framework has been largely used to solve autonomous target search and tracking [3], often relying on probabilistic approaches [4]: data from on-board sensors and Recursive Bayesian Estimation (RBE) schemes [5] are used to generate a probabilistic map (also known as belief map), encoding the knowledge about potential target locations. The control problem is then cast as the optimization of a suitable objective function built upon the probabilistic map (e.g., time to detection [2], estimate uncertainty [3], distance to the target [6]). Stochastic motion and observation models [1] account for the uncertainties on target dynamics and on the perception process, and allow to treat no-detection observations [7]. For these reasons, probabilistic approaches are suitable for real-life scenarios, which are also characterized by energy costs associated to the movement of the active sensing platform [8].

**Related works** - Typical modalities for active sensing include vision, audio and radio [1], [3], [9]. Visual-based tracking provides high accuracy [10] and does not require the target to use any emitting device. Occlusions and

Field of View (FoV) directionality [11] limit the range, applicability and success of camera-only platforms [4], especially for applications where time of detection is critical (e.g., search and rescue missions [12]). To collect measurements on wider ranges, and reduce the search phase, other technologies can be used, such as acoustic [9] or radio-frequency (RF) [3] signals. Despite the high localization accuracy of acoustic signals [9], sound pollution and extra hardware requirements (e.g., microphone arrays) are critical pitfalls of this technology [13]. Conversely, RF signals are energy efficient, have large reception ranges ( $\sim 100$  [m]), and low hardware requirements, since platforms are not needed to be equipped with multiple receivers; moreover, the Received Signal Strength Indicator (RSSI) is extracted from standard data packet traffic [14]. For these reasons, RSSI-based localization systems widely appear in literature and in commercial applications, despite environmental interference (e.g., cluttering and multi-path distortions) often limits their accuracy [14]. Multi-modal sensor fusion techniques have been shown to overcome the inadequacies of uni-modal approaches, being more robust and reliable [15].

**Contributions** - This paper exploits the complementary benefits of radio and visual cues for visually detecting a radio-emitting target with an aerial robot, equipped with a radio receiver and a Pan-Tilt (PT) camera. We formulate the control problem within a probabilistic active sensing framework, where camera measurements refine radio ones within a RBE scheme, used to keep the map updated. The fusion of RF and camera sensor data for target search and tracking is an open problem and the literature addressing this task is sparse. Indeed, to the best of authors knowledge, this is the first attempt to combine radio and visual measurements within a probabilistic active sensing framework. Furthermore, unlike existing solutions operating on limited control spaces (e.g., platform position [3] or camera orientation [15]), we propose a gradient-based optimal control, defined on a continuous space comprising both platform position and camera orientation. Theoretical and numerical analyses are provided to validate the effectiveness of the proposed algorithm. What emerges is that bi-modality is proven to increase the target localization accuracy; this, together with the availability of an integrated high-dimensional control space, leads to higher detection success rates, as well as superior time and energy efficiency with respect to radio and vision-only counterparts.

<sup>1</sup>L. Varotto and A. Cenedese are with the Department of Information Engineering, University of Padova, Italy. Corresponding author: [luca.varotto.5@phd.unipd.it](mailto:luca.varotto.5@phd.unipd.it).

<sup>2</sup>A. Cavallaro is with the Centre for Intelligent Sensing, Queen Mary University of London, U.K.

This work was partially supported by the Department of Information Engineering under the BIRD-SEED TSTARK project and by the Gini Foundation of the University of Padova.

## II. PROBLEM STATEMENT

Fig. 1 shows the main elements of the problem scenario, namely the target and the sensing platform<sup>1</sup>.

**Target** - The radio-emitting target moves on a planar environment  $\Pi \subset \mathbb{R}^2$ , according to a (possibly) non-linear stochastic Markovian state transition model [1]

$$\mathbf{p}_{t+1} = f(\mathbf{p}_t, \boldsymbol{\eta}_t). \quad (2)$$

where  $\mathbf{p}_t \in \Pi$  is the target position at time  $t$ , referred to the global 3D reference frame  $\mathcal{F}_0$ ; when expressed in  $\mathbb{R}^3$ , it is referred as  $\mathbf{p}_t^+ = [\mathbf{p}_t^\top \ 0]^\top$ . The uncertainty on the underlying target movements are captured by the distribution of the stochastic process noise  $\boldsymbol{\eta}_t$ . The probabilistic form of (2), namely  $p(\mathbf{p}_{t+1}|\mathbf{p}_t)$ , is known as process model [1].

**Sensing platform** - The sensing platform is an aerial vehicle (UAV), equipped with an omnidirectional radio receiver and a PT camera on gimbal, and endowed with processing capabilities and a real-time target detector [16]. The state of the platform is the camera pose, namely

$$\mathbf{s}_t = [\mathbf{c}_t^\top \ \boldsymbol{\psi}_t^\top]^\top, \quad (3)$$

$$\mathbf{c}_t \in \mathbb{R}^3; \quad \boldsymbol{\psi}_t = [\alpha_t \ \beta_t]^\top \in [-\pi/2 + \theta, \pi/2 - \theta]^2.$$

The UAV position  $\mathbf{c}_t$  is referred to  $\mathcal{F}_0$ , it is supposed to coincide with the camera focal point and its altitude is fixed (i.e., non-controllable);  $\alpha_t$  (resp.  $\beta_t$ ) is the pan (resp. tilt) angle w.r.t. the camera inertial reference frame  $\mathcal{F}_u$  (obtained by a  $\mathbf{c}_t$  translation of  $\mathcal{F}_0$ );  $\theta$  is the half-angle of view. The camera state follows a linear deterministic Markovian transition model [1]

$$\mathbf{s}_{t+1} = \mathbf{s}_t + \mathbf{u}_t; \quad \mathbf{u}_t = [\mathbf{u}_{\mathbf{c},t}^\top \ \mathbf{u}_{\boldsymbol{\psi},t}^\top]^\top \in \mathcal{A} \quad (4)$$

where  $\mathcal{A}$  is the control space. It comprises all possible control inputs that can be applied to the platform to regulate position and attitude. In particular, being the UAV altitude fixed, we focus on a planar control  $\mathbf{u}_{\mathbf{c}\Pi,t}$ , acting on the projection  $\mathbf{c}_{\Pi,t}$ . Inspired by real-life scenarios, the UAV movements are considered energy-consuming with a linear dependence on the flying distance [8], that is

$$\Delta E_t = d(\mathbf{c}_{t+1}, \mathbf{c}_t), \quad (5)$$

where  $\Delta E_t$  is the energy used to move the platform from  $\mathbf{c}_t$  to  $\mathbf{c}_{t+1}$ . The total available energy is denoted as  $E_{tot}$ .

<sup>1</sup>Bold letters indicate (column) vectors, if lowercase, matrices otherwise. With  $\mathbf{I}_n$  we define the  $n$ -dimensional identity matrix, while  $\mathbf{0}_n$  is the zero vector of dimension  $n$ .

Regarding the statistical distributions used in this paper,  $\chi^2(n)$  denotes the chi-squared distribution with  $n$  degrees of freedom, and  $\mathcal{N}(x|\mu, \sigma^2)$  is the Gaussian distribution over the random variable  $x$  with expectation  $\mu$  and variance  $\sigma^2$ .

With the shorthand notation  $z_{t_0:t_1}$  we indicate a sequence of measurements from time instant  $t_0$  to  $t_1$ , namely  $\{z_k\}_{k=t_0}^{t_1}$ . The Euclidean distance between vectors  $\mathbf{a}, \mathbf{b} \in \mathbb{R}^n$  is denoted as

$$d(\mathbf{a}, \mathbf{b}) = \|\mathbf{a} - \mathbf{b}\|_2 = \left( \sum_{i=1}^n (a(i) - b(i))^2 \right)^{1/2} \quad (1)$$

where  $a(i)$  is the  $i$ -th component of  $\mathbf{a}$ . Given a plane  $\Pi$  and a vector  $\mathbf{a} \in \mathbb{R}^n$ , we denote as  $\mathbf{a}_\Pi$  the orthogonal projection of  $\mathbf{a}$  onto  $\Pi$ .

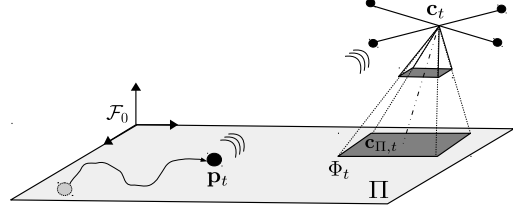


Fig. 1: Problem scenario. A target moves in a planar environment and establishes a radio signal communication with a camera-embedded UAV. The objective is to control the camera pose so that the target is visually detected.

Motivated by the long reception ranges of radio signals [14], we suppose the target to be always within the range of the platform receiver and, from received data packets, the RSSI value  $r_t \in \mathbb{R}$  is extracted. This is related to the platform-target distance  $d(\mathbf{c}_t, \mathbf{p}_t^+)$  according to the log-distance path loss model [17]

$$r_t = \kappa - 10n \log_{10} (d(\mathbf{c}_t, \mathbf{p}_t^+)). \quad (6)$$

The parameters  $\kappa$  and  $n$  are estimated via offline calibration procedures [14] and they represent the RSSI at a reference distance (e.g., 1 [m]) and the attenuation gain, respectively. Thus, defining  $T_{\text{RF}}$  as the receiver sampling interval, the radio observation model is

$$z_{\text{RF},t} = \begin{cases} r_t + v_{\text{RF},t}, & t = MT_{\text{RF}}, M \in \mathbb{N} \\ \emptyset, & \text{otherwise} \end{cases} \quad (7)$$

where  $v_{\text{RF},t} \sim \mathcal{N}(v|0, \sigma_{\text{RF}}^2)$  is the noise in RSSI measurements, and  $\emptyset$  is an empty observation (i.e., measurements without target information).

Camera measurements are modeled through the projection perspective geometry [10]

$$\mathbf{z}_{c,t} = \begin{cases} \mathbf{P}(\mathbf{s}_t) \tilde{\mathbf{p}}_t + \mathbf{v}_{c,t}, & D_t = 1 \text{ and } t = NT_a, N \in \mathbb{N} \\ \emptyset, & \text{otherwise} \end{cases} \quad (8)$$

where  $\mathbf{v}_t \sim \mathcal{N}(\mathbf{v}|\mathbf{0}_2, \boldsymbol{\Sigma}_c)$  is the noise of camera observations,  $\tilde{\mathbf{p}}_t$  is the homogeneous representation of  $\mathbf{p}_t^+$  and

$$\mathbf{P}(\mathbf{s}_t) = [\mathbf{I}_2 \ \mathbf{0}_2] \mathbf{K} [\mathbf{R}(\boldsymbol{\psi}_t) \ \mathbf{c}_t] \in \mathbb{R}^{2 \times 4} \quad (9)$$

is the camera projection matrix that maps  $\tilde{\mathbf{p}}_t$  onto the image plane  $\mathcal{I}$ .  $\mathbf{P}(\mathbf{s}_t)$  depends on  $\mathbf{K} \in \mathbb{R}^{3 \times 3}$ , the matrix of intrinsic parameters, and  $\mathbf{R}(\boldsymbol{\psi}_t)$ , the camera rotation matrix w.r.t.  $\mathcal{F}_0$ . The camera frame rate  $T_a$  satisfies

$$T_{\text{RF}} = \nu T_a, \quad \nu > 1 \quad (10)$$

since radio reception is typically characterized by longer sample rates than cameras [18], [19]. Without any loss of generality, we will consider a normalized frame rate (i.e.,  $T_a = 1$ ). Finally, a successful target detection is indicated by the value 1 of the binary variable  $D_t$ .

**Problem.** *With this formalism, the visual target detection problem can be formulated as the control of the camera state  $\mathbf{s}_t$  (through  $\mathbf{u}_t$ ) to realize event  $D_t$ .*

### III. METHODOLOGY

To solve the problem defined in Sec. II, a probabilistic bi-modal active sensing approach is proposed. As shown in Fig. 2, radio-visual measurements are aggregated to form a bi-modal likelihood function; this is used to keep the target belief map updated through an RBE scheme. Finally, an optimal controller is fed with the probabilistic map and generates the platform control input.

**Probabilistic map** - Given the observations  $\mathbf{z}_{1:t}$ , RBE provides a two-stage procedure to recursively update the target belief state, namely the posterior distribution  $p(\mathbf{p}_t|\mathbf{z}_{1:t})$ . The prediction stage involves using the process model (2) to obtain the prior of the target position via the Chapman-Kolmogorov equation [1]

$$p(\mathbf{p}_t|\mathbf{z}_{1:t-1}) = \int p(\mathbf{p}_t|\mathbf{p}_{t-1})p(\mathbf{p}_{t-1}|\mathbf{z}_{1:t-1})d\mathbf{p}_{t-1}. \quad (11)$$

As a new observation  $\mathbf{z}_t$  becomes available, Bayes rule [5] updates the target belief state

$$p(\mathbf{p}_t|\mathbf{z}_{1:t}) = \frac{p(\mathbf{p}_t|\mathbf{z}_{1:t-1})p(\mathbf{z}_t|\mathbf{p}_t)}{\int p(\mathbf{z}_t|\mathbf{p}_{t-1})p(\mathbf{p}_{t-1}|\mathbf{z}_{1:t-1})d\mathbf{p}_{t-1}}, \quad (12)$$

with  $p(\mathbf{p}_0)$  as initial target state belief.

Particle filtering [5] is a Monte Carlo approximation of the density  $p(\mathbf{p}_t|\mathbf{z}_{1:t})$  with a sum of  $N_s$  Dirac functions centered in the particles  $\{\mathbf{p}_t^{(i)}\}_{i=1}^{N_s}$ , that is

$$p(\mathbf{p}_t|\mathbf{z}_{1:t}) \approx \sum_{i=1}^{N_s} w_t^{(i)} \delta(\mathbf{p}_t - \mathbf{p}_t^{(i)}), \quad (13)$$

where  $w_t^{(i)}$  is the weight of particle  $\mathbf{p}_t^{(i)}$  and it holds

$$\mathbf{p}_t^{(i)} = f(\mathbf{p}_{t-1}^{(i)}, \boldsymbol{\eta}_{t-1}) \quad (14a)$$

$$w_t^{(i)} \propto w_{t-1}^{(i)} p(\mathbf{z}_t|\mathbf{p}_t^{(i)}) \quad (14b)$$

for  $i = 1, \dots, N_s$ . The  $i$ -th weight is therefore proportional to the likelihood function evaluated on the  $i$ -th particle, namely  $p(\mathbf{z}_t|\mathbf{p}_t^{(i)})$ . Under this scheme, a few particles will concentrate most of the weight over time, leading to a phenomenon called degeneracy. To alleviate this problem, systematic resampling is adopted, which involves resampling from the particle set. Particles with higher weights are more likely to be sampled, but the procedure preserves some low weight particles as well [5].

**Bi-modal likelihood** - In active sensing frameworks, the configuration of the sensing robot is not constant; hence, the likelihood function  $p(\mathbf{z}_t|\mathbf{p}_t)$  should account also for the platform state, that is  $p(\mathbf{z}_t|\mathbf{p}_t, \mathbf{s}_t)$ . Given this premise, and recalling the stochastic characterization of the radio observation model (7), the *RF likelihood* is

$$p(z_{\text{RF},t}|\mathbf{p}_t, \mathbf{s}_t) = \begin{cases} \mathcal{N}(z|r_t, \sigma_{\text{RF}}^2), & t = MT_{\text{RF}} \\ 1, & \text{otherwise.} \end{cases} \quad (15)$$

Note that  $z_{\text{RF},t}$  updates the belief map only when it carries information on the target position (i.e.,  $z_{\text{RF},t} \neq \emptyset$ , at  $t = MT_{\text{RF}}$ ).

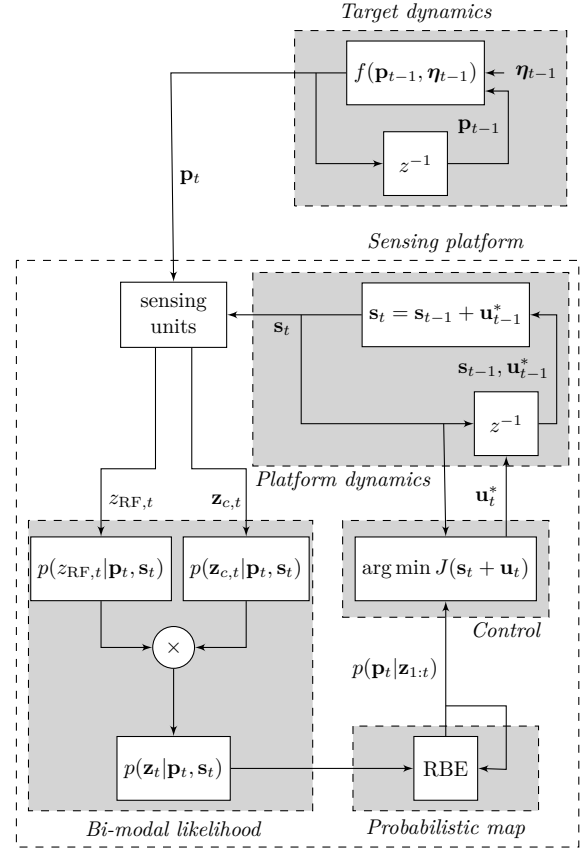


Fig. 2: Scheme of the proposed Probabilistic Radio-Visual Active Sensing algorithm.

To define the visual likelihood from the observation model (8), we consider the detection event as a Bernoulli random variable with success probability

$$p(D_t = 1|\mathbf{p}_t, \mathbf{s}_t) = \begin{cases} \Upsilon(\mathbf{p}_t, \mathbf{s}_t), & \mathbf{p}_t \in \Phi(\mathbf{s}_t) \\ 0, & \text{otherwise} \end{cases} \quad (16)$$

with  $\Phi(\mathbf{s}_t)$  camera FoV onto  $\Pi$  (see Fig. 1), and

$$\Upsilon(\mathbf{p}_t, \mathbf{s}_t) = \left[ 1 + e^{\gamma(d(\mathbf{c}_t, \mathbf{p}_t^+)/f - \epsilon)} \right]^{-1} (1 + e^{-\gamma\epsilon}). \quad (17)$$

Thus, the target can be detected only if inside the camera FoV and, from (17), the detection probability is proportional to the resolution  $d(\mathbf{c}_t, \mathbf{p}_t^+)/f$  at which the target is observed, where  $f$  is the camera focal length;  $\epsilon > 0$  is the resolution at which the target is no longer well detectable,  $\gamma > 0$  is the rate of the target detectability decrease. Then, the *visual likelihood* is

$$p(\mathbf{z}_{c,t}|\mathbf{p}_t, \mathbf{s}_t) = p(\mathbf{z}_{c,t}|\mathbf{p}_t, \mathbf{s}_t, D_t)p(D_t|\mathbf{p}_t, \mathbf{s}_t) = \begin{cases} \mathcal{N}(\mathbf{z}|\mathbf{P}(\mathbf{s}_t)\tilde{\mathbf{p}}_t, \boldsymbol{\Sigma}_c)\Upsilon(\mathbf{p}_t, \mathbf{s}_t), & D_t = 1, \mathbf{p}_t \in \Phi(\mathbf{s}_t) \\ 0, & D_t = 1, \mathbf{p}_t \notin \Phi(\mathbf{s}_t) \\ 1 - \Upsilon(\mathbf{p}_t, \mathbf{s}_t), & D_t = 0, \mathbf{p}_t \in \Phi(\mathbf{s}_t) \\ 1, & D_t = 0, \mathbf{p}_t \notin \Phi(\mathbf{s}_t) \end{cases} \quad (18)$$

By aggregating radio and visual likelihoods, the following *bi-modal likelihood* is obtained

$$p(\mathbf{z}_t | \mathbf{p}_t, \mathbf{s}_t) = p(z_{\text{RF},t} | \mathbf{p}_t, \mathbf{s}_t) p(\mathbf{z}_{c,t} | \mathbf{p}_t, \mathbf{s}_t). \quad (19)$$

Then, (19) is applied to the update stage (14b) of the particle filter that implements the RBE scheme.

**Controller** - The platform control input is computed by solving the following optimization program

$$\begin{aligned} \mathcal{C} : \mathbf{u}_t^* &= \arg \min_{\mathbf{u}_t \in \mathcal{A}} J(\mathbf{s}_t + \mathbf{u}_t) \\ \text{s.t. } &d(\mathbf{c}_{t+1}, \mathbf{c}_t) \leq E_t \end{aligned} \quad (20)$$

where  $E_t$  is the residual energy at time  $t$ , computed as

$$E_t = E_{\text{tot}} - \sum_{k=0}^{t-1} \Delta E_k = E_{\text{tot}} - \sum_{k=0}^{t-1} d(\mathbf{c}_{k+1}, \mathbf{c}_k). \quad (21)$$

The cost function is chosen as

$$J(\mathbf{c}_{\Pi,t+1}) = \frac{1}{2} d(\mathbf{c}_{\Pi,t+1}, \hat{\mathbf{p}}_t)^2, \quad (22)$$

where  $\mathbf{c}_{\Pi,t+1}$  is the projection of  $\mathbf{c}_{t+1}$  onto  $\Pi$ , and  $\hat{\mathbf{p}}_t$  is the MAP estimate<sup>2</sup> of the target position; formally

$$\hat{\mathbf{p}}_t = \mathbf{p}_t^{(i^*)}; \quad i^* = \arg \max_{i \in [1, N_s]} w_t^{(i)}. \quad (23)$$

Note that  $J(\cdot)$  is function of  $\mathbf{s}_t + \mathbf{u}_t$  (i.e.,  $\mathbf{s}_{t+1}$ ), since  $\mathbf{c}_{\Pi,t+1}$  can be regulated by acting on the camera pose, through the inverse perspective geometry (with known and fixed UAV altitude w.r.t.  $\Pi$ ) [10]. Furthermore,  $J(\cdot)$  extracts information from the belief map, according to the probabilistic active sensing approach (Fig. 2).

The convexity of  $J(\cdot)$  w.r.t.  $\mathbf{c}_{\Pi,t+1}$  allows to solve (20) with the gradient-based control law

$$\begin{cases} \mathbf{s}_{\tau+1} = \mathbf{s}_\tau + \mathbf{u}_\tau, \quad \tau \in [0, \tau_{\text{max}}] \\ \mathbf{u}_\tau = \begin{bmatrix} \mathbf{u}_{c,t} \\ \mathbf{u}_{\psi,t} \end{bmatrix} = - \begin{bmatrix} \mathbf{G}_c & \mathbf{0} \\ \mathbf{0} & \mathbf{G}_\psi \end{bmatrix} \begin{bmatrix} \frac{\partial J(\mathbf{c}_{\Pi,\tau+1})}{\partial \mathbf{c}_\Pi} \\ 0 \\ \frac{\partial J(\mathbf{c}_{\Pi,\tau+1})}{\partial \psi} \end{bmatrix} \end{cases} \quad (24)$$

where  $\tau_{\text{max}}$  accounts for the maximum number of iterations in order to accommodate the next incoming measurement at  $t+1$ .  $\mathbf{G}_c \in \mathbb{R}^{3 \times 3}$  and  $\mathbf{G}_\psi \in \mathbb{R}^{2 \times 2}$  are suitable control gain matrices. By choosing  $\mathbf{G}_c$  entries small, energy is preserved, since (24) commands short UAV movements. Conversely, larger  $\mathbf{G}_c$  and  $\mathbf{G}_\psi$  lead to a more reactive system, capable of getting close to the setpoint  $\hat{\mathbf{p}}_t$  within a maximum number of iterations  $\tau_{\text{max}}$ . Consequently, if the localization procedure is accurate (i.e.,  $\hat{\mathbf{p}}_t \approx \mathbf{p}_t$ ), the condition  $\mathbf{p}_t \in \Phi(\mathbf{s}_t)$  is likely to be satisfied and  $d(\mathbf{c}_t, \mathbf{p}_t^+)$  is small, which is necessary to have high detection probabilities, according to (16). Finally, it is important to remark that  $J(\cdot)$  is *purely-exploitative*

<sup>2</sup>An alternative would be the MMSE estimate [6], namely  $\hat{\mathbf{p}}_t = \sum_{i=1}^{N_s} \omega_t^{(i)} \mathbf{p}_t^{(i)}$ . This choice leads to smoother trajectories, but it is proven to make  $\mathcal{C}$  more prone to local minima [1].

and *not energy-aware*: in the controller design problem  $\mathcal{C}$ , energy appears only in the constraint and no energy preservation [8], nor information-seeking (explorative) [1] criteria are included.

#### IV. THEORETICAL RESULTS

This Section formally motivates the use of an action space involving the entire camera pose, as in (4), and supports the choice of a combined radio-visual perception system. We observe that the particle weight distribution is an indicator of the target localizability: highly-weighted regions allow to focus the position estimate, while uniform weight patterns suggest ambiguity in the target localization. In this respect, we show that radio-only solutions need the sensing platform to move in order to solve localization ambiguity (Ths. 1-2 that follow), which can be conversely attained through a radio-visual approach also with a static platform (Th. 3).

**Theorem 1.** *Let the following hypotheses hold*

- 1) *the target moves according to an unbiased random walk, i.e.,  $p(\mathbf{p}_{t+1} | \mathbf{p}_t) = \mathcal{N}(\mathbf{p} | \mathbf{p}_t, \sigma^2 \mathbf{I}_2)$ ;*
- 2) *the platform is static, i.e.  $\mathbf{c}_t = \mathbf{c}$ ;  $\forall t$ ;*
- 3) *the RBE scheme updates through (14b) exploiting only the RF likelihood (15).*

Then,

$$\begin{aligned} \mathbb{E} \left[ \omega_t^{(i)} | z_{\text{RF},1:t} \right] &= \mathbb{E} \left[ \omega_t^{(j)} | z_{\text{RF},1:t} \right], \quad t \geq 0 \\ \forall i, j \in [1, \dots, N_s] \text{ s.t. } &d(\mathbf{p}_0^{(i)}, \mathbf{c}_\Pi) = d(\mathbf{p}_0^{(j)}, \mathbf{c}_\Pi) \end{aligned} \quad (25)$$

*Proof.* The dynamic model associated to the target unbiased random walk is

$$\mathbf{p}_{t+1} = \mathbf{p}_t + \boldsymbol{\eta}_t, \quad \boldsymbol{\eta}_t \sim \mathcal{N}(\boldsymbol{\eta} | \mathbf{0}_2, \sigma^2 \mathbf{I}_2) \quad (26)$$

Equivalently,

$$\mathbf{p}_t = \mathbf{p}_0 + \sum_{k=0}^{t-1} \boldsymbol{\eta}_k, \quad t > 0. \quad (27)$$

Given  $\boldsymbol{\eta}_t, \boldsymbol{\eta}_s$  i.i.d. for any  $s \neq t$ , it follows

$$\bar{\boldsymbol{\eta}}_{t-1} := \sum_{k=0}^{t-1} \boldsymbol{\eta}_k \sim \mathcal{N}(\boldsymbol{\eta} | \mathbf{0}_2, t\sigma^2 \mathbf{I}_2). \quad (28)$$

Then, the squared distance  $d_t^{(i),2} := d(\mathbf{p}_t^{(i)}, \mathbf{c}_\Pi)^2$  is

$$\begin{aligned} d_t^{(i),2} &= \|\mathbf{p}_t^{(i)} - \mathbf{c}_\Pi\|_2^2 = \|\mathbf{p}_0^{(i)} + \bar{\boldsymbol{\eta}}_{t-1} - \mathbf{c}_\Pi\|_2^2 \\ &= \sum_{\ell=1}^2 \left( p_0^{(i)}(\ell) - c_\Pi(\ell) \right)^2 + \sum_{\ell=1}^2 \bar{\eta}_{t-1}(\ell)^2 \\ &\quad + 2 \sum_{\ell=1}^2 \left( p_0^{(i)}(\ell) - c_\Pi(\ell) \right) \bar{\eta}_{t-1}(\ell), \quad t > 0. \end{aligned} \quad (29)$$

It holds,

$$2 \left( p_0^{(i)}(\ell) - c_\Pi(\ell) \right) \bar{\eta}_{t-1}(\ell) \sim \mathcal{N} \left( \boldsymbol{\eta} | \mathbf{0}, 4t\sigma^2 \left( p_0^{(i)}(\ell) - c_\Pi(\ell) \right)^2 \right) \quad (30)$$

and, since the components of  $\bar{\boldsymbol{\eta}}_{t-1}$  are i.i.d. with distribution  $\mathcal{N}(0, t\sigma^2)$ ,

$$\sum_{\ell=1}^2 \bar{\eta}_{t-1}(\ell)^2 \sim t\sigma^2 \chi^2(2). \quad (31)$$

Finally, recalling that  $\sum_{\ell=1}^2 (p_0^{(i)}(\ell) - c_{\Pi}(\ell))^2 = d_0^{(i)}$ ,

$$d_t^{(i),2} \sim \mathcal{N}(d^2|\mu_d, \sigma_d^2) + t\sigma^2 \chi^2(2), \quad t \geq 0 \quad (32)$$

with

$$\mu_d = d_0^{(i),2}, \quad \sigma_d^2 = 4t\sigma^2 d_0^{(i),2}. \quad (33)$$

From (32)-(33),  $d_t^{(i),2}$  is identically distributed for all particles with the same initial distance from the platform. Using likelihood (15) and with  $z_{\text{RF},1:t}$  given,  $\omega_t^{(i)}$  is a (non-linear) function of  $d_t^{(i),2}$ , through (6). Then, condition (25) follows.  $\square$

**Theorem 2.** *Let the following hypotheses hold*

- 1) *the target moves according to an unbiased random walk, i.e.,  $p(\mathbf{p}_{t+1}|\mathbf{p}_t) = \mathcal{N}(\mathbf{p}|\mathbf{p}_t, \sigma^2 \mathbf{I}_2)$ ;*
- 2) *the platform moves at a fixed altitude according to a deterministic linear Markovian motion, i.e.,  $\mathbf{c}_{\Pi,t+1} = \mathbf{c}_{\Pi,t} + \mathbf{u}_{\mathbf{c}_{\Pi,t}}$ ;*
- 3) *the RBE scheme updates through (14b) exploiting only the RF likelihood (15).*

Then,

$$\begin{aligned} &\exists(i, j) \in [1, N_s] \text{ s.t. } d(\mathbf{p}_0^{(i)}, \mathbf{c}_{\Pi,0}) = d(\mathbf{p}_0^{(j)}, \mathbf{c}_{\Pi,0}) \text{ and} \\ &\mathbb{E} \left[ \omega_t^{(i)} | z_{\text{RF},1:t} \right] \neq \mathbb{E} \left[ \omega_t^{(j)} | z_{\text{RF},1:t} \right], \quad t > 0 \end{aligned} \quad (34)$$

*Proof.* The platform planar dynamics can be equivalently written as

$$\mathbf{c}_{\Pi,t} = \mathbf{c}_{\Pi,0} + \bar{\mathbf{u}}_{t-1}, \quad \bar{\mathbf{u}}_{t-1} := \sum_{k=0}^{t-1} \mathbf{u}_{\mathbf{c}_{\Pi,k}}, \quad t > 0. \quad (35)$$

With similar computations involved of Th. 1, it is possible to show that the squared distance  $d_t^{(i),2} := d(\mathbf{p}_t^{(i)}, \mathbf{c}_{\Pi,t})^2$  is distributed as

$$d_t^{(i),2} \sim \mathcal{N}(d^2|\mu_d, \sigma_d^2) + t\sigma^2 \chi^2(2, \lambda), \quad t > 0 \quad (36)$$

with

$$\begin{aligned} \mu_d &= d_0^{(i),2} - 2(\mathbf{p}_0^{(i)} - \mathbf{c}_{\Pi,0})^\top \bar{\mathbf{u}}_{t-1}, \quad \sigma_d^2 = 4t\sigma^2 d_0^{(i),2} \\ \lambda &= - \sum_{\ell=1}^2 \bar{u}_{\mathbf{c}_{\Pi,t-1}}(\ell)^2 \end{aligned} \quad (37)$$

where  $\chi^2(2, \lambda)$  is a non-central chi-squared distribution, with non-centrality parameter  $\lambda$ . From (36)-(37), the distribution of  $d_t^{(i),2}$  depends on both  $d_0^{(i),2}$  and  $(\mathbf{p}_0^{(i)} - \mathbf{c}_{\Pi,0})^\top \bar{\mathbf{u}}_{t-1}$ . It is always possible to find  $(i, j) \in [1, N_s]$ , such that  $d_0^{(i)} = d_0^{(j)}$  and  $(\mathbf{p}_0^{(i)} - \mathbf{c}_{\Pi,0})^\top \bar{\mathbf{u}}_{t-1} \neq (\mathbf{p}_0^{(j)} - \mathbf{c}_{\Pi,0})^\top \bar{\mathbf{u}}_{t-1}$ . Then, in general,

$$\mathbb{E} \left[ \omega_t^{(i)} | z_{\text{RF},1:t} \right] \neq \mathbb{E} \left[ \omega_t^{(j)} | z_{\text{RF},1:t} \right]. \quad (38) \quad \square$$

**Theorem 3.** *Let the following hypotheses hold*

- 1) *the target moves according to an unbiased random walk, i.e.,  $p(\mathbf{p}_{t+1}|\mathbf{p}_t) = \mathcal{N}(\mathbf{p}|\mathbf{p}_t, \sigma^2 \mathbf{I}_2)$ ;*
- 2) *the platform is static, i.e.  $\mathbf{c}_t = \mathbf{c}$ ;  $\forall t$ ;*
- 3) *the RBE scheme updates through (14b) exploiting the radio-visual likelihood (19).*

Then,

$$\begin{aligned} &\exists(i, j) \in [1, N_s] \text{ s.t. } d(\mathbf{p}_0^{(i)}, \mathbf{c}_{\Pi}) = d(\mathbf{p}_0^{(j)}, \mathbf{c}_{\Pi}) \text{ and} \\ &\mathbb{E} \left[ \omega_t^{(i)} | z_{\text{RF},1:t} \right] \neq \mathbb{E} \left[ \omega_t^{(j)} | z_{\text{RF},1:t} \right], \quad t > 0 \end{aligned} \quad (39)$$

*Proof.* Suppose (w.l.o.g.) that  $\mathbf{p}_0^{(i)}$  and  $\mathbf{p}_0^{(j)}$  satisfy  $d(\mathbf{p}_0^{(i)}, \mathbf{c}_{\Pi}) = d(\mathbf{p}_0^{(j)}, \mathbf{c}_{\Pi})$ ; hence,  $d_t^{(i),2}$  and  $d_t^{(j),2}$  are equally distributed, from Th. 1. Suppose now that  $\mathbf{p}_t^{(i)} \in \Phi(\mathbf{s}_t)$ , but  $\mathbf{p}_t^{(j)} \notin \Phi(\mathbf{s}_t)$ . From (18)-(19),  $\omega_t^{(i)}$  and  $\omega_t^{(j)}$  are different functions of two equally distributed random variables (once  $z_{\text{RF},1:t}$  are fixed). Thus, in general,  $\mathbb{E} \left[ \omega_t^{(i)} | z_{\text{RF},1:t} \right] \neq \mathbb{E} \left[ \omega_t^{(j)} | z_{\text{RF},1:t} \right]$ .  $\square$

#### A. Discussion

Th. 1 statistically characterizes the axis-symmetric ambiguity, one of the main issues of RSSI-based localization systems. As (6) suggests, RSSI values bring information only on the target-receiver distance; consequently, the RF likelihood (15) is axis-symmetric w.r.t. the receiver. Thus, in a particle-based RBE scheme, particles at the same distance from the receiver are equally weighted. When the sensing platform is static, this phenomenon generates severe convergence issues, since the belief map is toroidal with non-unique MAP estimate, as depicted in Fig. 3(a). For this reason, most literature solutions propose to use multiple receivers [20]. When this is not feasible, the axis-symmetric effect can be mitigated by using a single moving receiver, as proven in Th. 2. Therefore, including the platform position in the control space, as in (4), is beneficial for the convergence of RSSI-based probabilistic active tracking strategies. Another viable solution is the adoption of a bi-modal perception system. According to Th. 3, the visual likelihood (18) reduces the ambiguity in the particles weighting process. This is one main advantage of the radio-visual approach w.r.t. the radio-only counterpart. To completely exploit the disambiguation effect of visual observations, camera orientation should be included in the control space, as in (4). In particular, with the control law defined in Sec. III, the platform uses camera measurements to discard wrong MAP candidates. In this way, most of the weight will concentrate around the true target position over time, as Fig. 3(b) shows.

In conclusion, combining radio-visual cues in the RBE scheme and comprising the entire camera pose in  $\mathcal{A}$ , reduces the estimation ambiguities. This makes the localization procedure faster and more accurate (Sec. IV-B). Accordingly, the overall target visual detection task becomes more robust and more efficient (Sec. V).

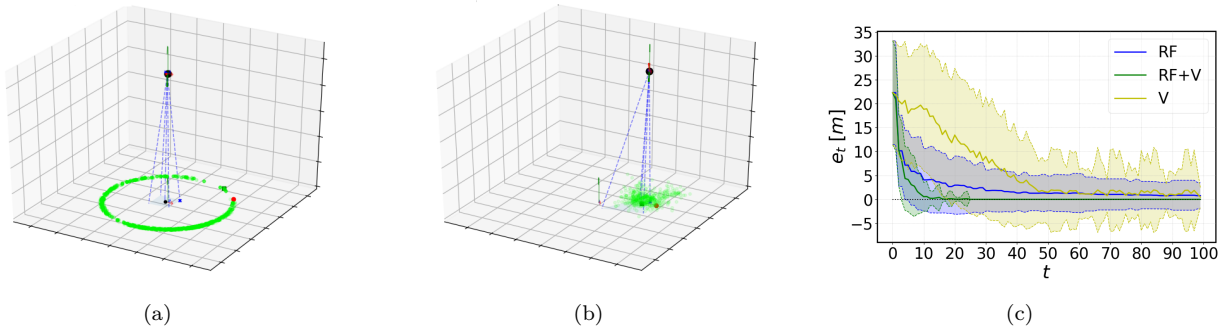


Fig. 3: Probabilistic map obtained with the uni-modal RF likelihood (a) and the bi-modal radio-visual likelihood (b). (c) Localization error (average and 68% confidence interval over a MC simulation) with radio-only (RF), visual-only (V) and radio-visual (RF+V) likelihood.

### B. Proof of concept - target localization

To support the theoretical results, the control law (20) is used to localize a static target (i.e.,  $\mathbf{p}_t = \mathbf{p}; \forall t$ ) in a Python-based synthetic environment (see Fig. 3). For consistency with the hypotheses of Th. 1-3, the process model is an unbiased random walk. The receiver is kept static (i.e.,  $\mathbf{G}_c = \mathbf{0}$ ), to stress the effects of the axis-symmetric ambiguity, as well as the improvements introduced by visual information. RSSI data are collected with sampling rate  $T_{\text{RF}} = 2$  ( $T_a = 1$ ) and noise level  $\sigma_{\text{RF}} = 2$  [dBm]; the target is placed at distance  $d(\mathbf{p}^+, \mathbf{c}) = 10$  [m] from the platform. The proposed bi-modal radio-visual approach (RF+V) is compared with a visual-only (V) and a radio-only (RF) one. To capture the performance variability, the evaluation is assessed through a Monte Carlo (MC) simulation with  $N_{\text{tests}} = 150$  tests of  $T_W = 100$  iterations each. The performance index is the localization error  $e_t = d(\mathbf{p}, \hat{\mathbf{p}}_t)$ .

Fig. 3(c) depicts the average localization error and its 68% confidence interval over the MC tests. Only RF+V converges to the groundtruth; namely, the estimate is unbiased and with zero variability over the MC tests

$$\begin{aligned} \mu_{e_{T_W}} &:= \mathbb{E}[e_{T_W}] = 0 \text{ [m]} \\ \sigma_{e_{T_W}}^2 &:= \mathbb{E}[(e_{T_W} - \mu_{e_{T_W}})^2] = 0 \text{ [m]}. \end{aligned} \quad (40)$$

The effect of the axis-symmetric ambiguity is clear in the RF approach. As proven in Th. 1, the MAP estimate is non-unique; hence, at any time, the estimate  $\hat{\mathbf{p}}_t$  may be not representative of the true target position. This leads RF to converge, on average, to a biased estimate ( $\mu_{e_{T_W}} \approx 1$  [m]), with remarkable inter-test variability ( $\sigma_{e_{T_W}} \approx 3$  [m]). The oscillations of  $e_t$  are even higher for the visual-only approach. The main issue here is related to the limited sensing domain of the camera: as (18) suggests, in case of non-detection ( $D_t = 0$ ), only particles inside the camera FoV are updated; these might be a small portion of the entire particles set. Consequently, many particles share the same weight for a long time, leading to a stronger ambiguity than the axis-symmetry (especially in the first iterations). Therefore, the localization procedure experiences a very slow and

erratic converge behavior.

## V. NUMERICAL RESULTS

In this Section the localization problem of Sec. IV-B is extended to the active tracking of a moving target. At first, we numerically motivate the choice of the entire camera pose as control space (Sec. V-C), in accordance with the theoretical results of Sec. IV. Secondly, we show that bi-modality allows to achieve higher robustness and time-efficiency than several uni-modal baselines (Sec. V-D). Finally, the proposed algorithm is proven to be even more energy-efficient than a radio-only counterpart (Sec. V-E), albeit the control law (20) does not account for any energy-preserving term.

### A. Setup parameters

As in Sec. IV-B, we compare RF+V, RF and V over a MC simulation with  $N_{\text{tests}} = 150$  tests of  $T_W = 100$  iterations each. The belief map is approximated by  $N_s = 500$  particles, initialized according to a uniform distribution over  $\Pi$ . The underlying target motion is simulated using a linear stochastic Markovian transition planar model

$$\mathbf{p}_{t+1} = \mathbf{p}_t + \mathbf{q}_t; \quad \mathbf{q}_t \sim \mathcal{N}(\mathbf{q}|\boldsymbol{\mu}_q, \boldsymbol{\Sigma}_q), \quad \boldsymbol{\mu}_q \neq \mathbf{0}_2. \quad (41)$$

The initial condition  $\mathbf{p}_0$  is randomly changed at each MC test, as well as the platform initial planar position  $\mathbf{c}_{\Pi,0}$ . The process model is an unbiased random walk, the receiver sampling rate is  $T_{\text{RF}} = 10$  ( $T_a = 1$ ), the total available energy is fixed to  $E_{\text{tot}} = 300$ , and the RSSI noise level is  $\sigma_{\text{RF}} = 3.5$  [dBm].

### B. Performance assessment

The performance assessment of the active tracking task is based on the following indices.

- 1) *Detection success rate*: robustness index that counts the number of successful target visual detections over the MC tests

$$\begin{aligned} \varpi &= \frac{1}{N_{\text{tests}}} \sum_{j=1}^{N_{\text{tests}}} \mathbb{1}_{D,j} \\ \mathbb{1}_{D,j} &= \begin{cases} 1, & \text{if } \exists t_D \in [1, T_W] \text{ s.t. } D_{t_D} = 1 \\ 0, & \text{otherwise} \end{cases} \end{aligned} \quad (42)$$

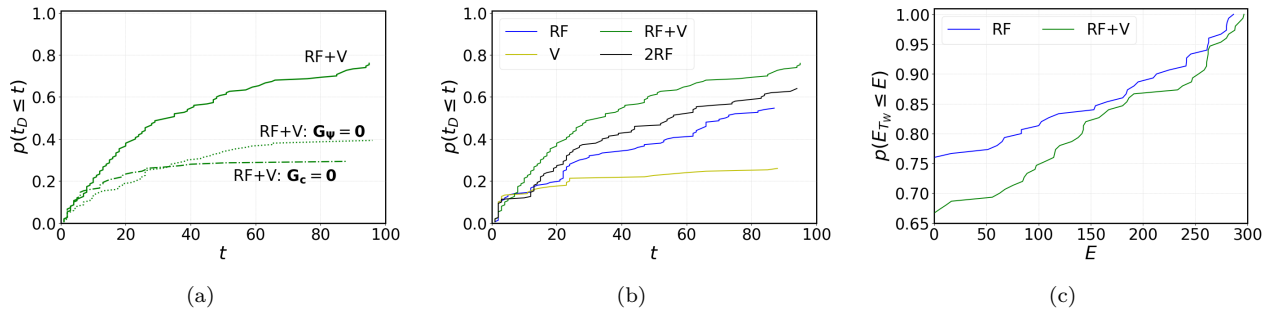


Fig. 4: MC simulation results. (a) Detection time ECDF with different control spaces: full camera pose (RF+V), no pan-tilt movements (RF+V:  $\mathbf{G}_\Psi = \mathbf{0}$ ), static platform (RF+V:  $\mathbf{G}_c = \mathbf{0}$ ). (b) Detection time ECDF with different type and amount of information employed for the tracking task: radio-visual (RF+V), visual-only (V), radio-only (RF), and radio-only with two receivers (2RF). (c) Energy consumption ECDF between RF+V and RF.

- 2) *Detection time ECDF*<sup>3</sup>: time-efficiency index that accounts for the time required to visually detect the target

$$p(t_D \leq t) = \frac{1}{N_{tests}} \sum_{j=1}^{N_{tests}} \mathbb{1}_{t_{D,j} \leq t} \quad (43)$$

$$\mathbb{1}_{t_{D,j} \leq t} = \begin{cases} 1, & \text{if } t_{D,j} \leq t \\ 0, & \text{otherwise} \end{cases}$$

- 3) *Energy consumption ECDF*: energy-efficiency index that accounts for the amount of available energy  $E_{TW} \in [0, E_{tot}]$  at the end of the task

$$p(E_{TW} \leq E) = \frac{1}{N_{tests}} \sum_{j=1}^{N_{tests}} \mathbb{1}_{E_{TW,j} \leq E} \quad (44)$$

$$\mathbb{1}_{E_{TW,j} \leq E} = \begin{cases} 1, & \text{if } E_{TW,j} \leq E \\ 0, & \text{otherwise.} \end{cases}$$

### C. Impact of the control space

The controller  $\mathcal{C}$ , described in Sec. III, acts on a high-dimensional space comprising the full camera pose (namely, its position and orientation). This choice has been theoretically motivated in Ths. 2-3 of Sec. IV and it is here supported by numerical results.

Specifically, the proposed control law (i.e., RF+V) is compared with two variants: the first does not allow pan-tilt movements (i.e.,  $\mathbf{G}_\Psi = \mathbf{0}$ ) and the camera is fixed and facing downwards (namely,  $\alpha_t = \beta_t = 0, \forall t$ ); the second considers a static platform (i.e.,  $\mathbf{G}_c = \mathbf{0}$ ). Indeed, without pan-tilt actuation, the target can be detected only when the UAV gets very close to it. However, this requirement is difficult to be met for every initial condition  $\mathbf{p}_0$  and  $\mathbf{c}_0$ , due to localization errors and to the bias in the target motion. On the other side, a static platform is not capable to get closer to the target; hence, according to (16)-(17), many detection failures may occur. These considerations are supported by the numerical results reported in Tab. I (top row): the

<sup>3</sup>ECDF: Empirical Cumulative Distribution Function.

TABLE I: Detection success rate of the compared approaches.

	RF+V	RF+V: $\mathbf{G}_\Psi = \mathbf{0}$	RF+V: $\mathbf{G}_c = \mathbf{0}$
$\varpi$	77%	39%	29%
	RF	V	2RF
$\varpi$	55%	26%	64%

detection success rate of RF+V is 77%, against 39% of the case  $\mathbf{G}_\Psi = \mathbf{0}$  and 29% of the case  $\mathbf{G}_c = \mathbf{0}$ . Moreover, Fig. 4(a) shows a remarkable difference in the detection time ECDF between the proposed solution and the other two versions. In conclusion, considering the entire camera pose as control space induces more robustness and more time-efficiency in the target visual detection task.

### D. Impact of the sensing modalities

As shown in Sec. IV-B, RF+V achieves a more accurate localization than than RF and V. This, combined with the control law  $\mathcal{C}$ , allows the platform to get closer to the target and to move the camera so that the target is inside the FoV. These two factors induce higher detection probabilities, according to (16)-(17). As a consequence, active tracking is more robust (see Tab. I) and more time-efficient (see Fig. 4(b)) when adopting the proposed bi-modal strategy, rather than the uni-modal counterparts.

One may argue that the superior performance of the bi-modal strategy is due to the larger amount of information involved. To this aim, we compared RF+V with 2RF: instead of combining radio-visual data (heterogeneous sensor fusion), we aggregate observations coming from two receivers (homogeneous radio-only sensor fusion). Thus, the measurements of 2RF are

$$\mathbf{z}_{2RF,t} = [z_{RF^{(1)},t} \quad z_{RF^{(2)},t}]^T \quad (45)$$

where  $z_{RF^{(\ell)},t}$  identifies the RSSI sample collected by the  $\ell$ -th receiver at time  $t$ , according to the model (7). Supposing independence between the observations of the two receivers, the likelihood of 2RF becomes

$$p(\mathbf{z}_{2RF,t} | \mathbf{p}_t, \mathbf{s}_t) = \prod_{\ell=1}^2 p(z_{RF^{(\ell)},t} | \mathbf{p}_t, \mathbf{s}_t), \quad (46)$$

with  $p(z_{\text{RF}(e),t}|\mathbf{p}_t, \mathbf{s}_t)$  as in (15). Tab. I and Fig. 4(b) show that 2RF is more robust and time-efficient than RF, but less than RF+V. This means that the tracking performance is not only affected by the *quantity*, but also by the *quality*, of the aggregated information. In particular, exploiting complementary cues (e.g. radio and visual ones) is more advantageous than combining homogeneous data extracted from different sources; in fact, one can prove that the axis-symmetric ambiguity is not reduced when applying multiple receivers placed at the same location.

### E. Energy-efficiency

As mentioned in Sec. III, the proposed control law (20) does not include any explicit energy-aware term; hence,  $\mathcal{C}$  is not expected to generate energy-preserving platform movements (unless  $\mathbf{G}_c$  is kept small, but this has been proven to be ineffective). Therefore, when the total available energy runs out, that is

$$\exists t \in [1, T_W] \text{ s.t. } E_t = 0, \quad (47)$$

the platform becomes static and the detection capabilities dramatically decrease (see Sec. V-C). In the absence of an energy-aware control technique, the only way to avoid energy run-out is by producing accurate target position estimates. In fact, if  $\hat{\mathbf{p}}_t \approx \mathbf{p}_t$ , the controller  $\mathcal{C}$  drives the platform towards the target through a smooth and direct trajectory, which is more energy-efficient than irregular patterns, according to (5).

Given this premise, and the localization superiority of RF+V w.r.t. RF (Secs. III and V-D), we expect to have more energy preservation in RF+V than in RF. Indeed, the two energy consumption ECDFs in Fig. 4(c) satisfy

$$p(E_{T_W}^{\text{RF+V}} \leq E) < p(E_{T_W}^{\text{RF}} \leq E); \forall E \in [0, E_{\text{tot}}]. \quad (48)$$

This means that RF drains more energy than RF+V. In particular, the out-of-energy condition (47) is higher in RF (76%) than in RF+V (68%).

## VI. CONCLUSION

This work discusses the problem of visually detecting a RF-emitting target under energy constraint. To this aim, we propose a probabilistic active sensing approach, leveraging radio-visual information.

A theoretical discussion highlights the main limitations of radio-only localization, as well as the benefits introduced by the bi-modal strategy. These findings are then validated through numerical results, from which bi-modality is shown to be more robust and more time and energy-efficient than uni-modal camera and radio-only counterparts. Bi-modality is proven to be even more effective than homogeneous sensor fusion strategies, since the combination of two receivers does not get comparable performance of the suggested radio-visual integration.

Future work will be devoted to the design of specific energy-aware terms to be included in the optimal controller design. In addition, it is worth comparing the

proposed exploitative strategy with information-seeking (explorative) ones. Finally, we are planning to carry out laboratory experiments to evaluate the algorithm on a real robotic platforms.

## REFERENCES

- [1] S. Radmard and E. A. Croft, "Active target search for high dimensional robotic systems," *Autonomous Robots*, vol. 41, no. 1, pp. 163–180, 2017.
- [2] S. Pérez-Carabaza, J. Scherer, B. Rinner, J. A. López-Orozco, and E. Besada-Portas, "Uav trajectory optimization for minimum time search with communication constraints and collision avoidance," *Engineering Applications of Artificial Intelligence*, vol. 85, pp. 357–371, 2019.
- [3] S. A. A. Shahidian and H. Soltanizadeh, "Single-and multi-uav trajectory control in rf source localization," *Arabian Journal for Science and Engineering*, vol. 42, no. 2, pp. 459–466, 2017.
- [4] C. Robin and S. Lacroix, "Multi-robot target detection and tracking: taxonomy and survey," *Autonomous Robots*, vol. 40, no. 4, pp. 729–760, 2016.
- [5] A. Smith, *Sequential Monte Carlo methods in practice*. Springer Science & Business Media, 2013.
- [6] M. Hasanzade, Ö. Herekoğlu, R. Yeniçeri, E. Koyuncu, and G. İnalan, "Rf source localization using unmanned aerial vehicle with particle filter," in *2018 9th International Conference on Mechanical and Aerospace Engineering (ICMAE)*. IEEE, 2018, pp. 284–289.
- [7] W. Koch, "On exploiting 'negative' sensor evidence for target tracking and sensor data fusion," *Information Fusion*, vol. 8, no. 1, pp. 28–39, 2007.
- [8] C. H. Liu, Z. Chen, J. Tang, J. Xu, and C. Piao, "Energy-efficient uav control for effective and fair communication coverage: A deep reinforcement learning approach," *IEEE Journal on Selected Areas in Communications*, vol. 36, no. 9, pp. 2059–2070, 2018.
- [9] T. Haubner, A. Schmidt, and W. Kellermann, "Active acoustic source tracking exploiting particle filtering and monte carlo tree search," in *2019 27th European Signal Processing Conference (EUSIPCO)*. IEEE, 2019, pp. 1–5.
- [10] H. Aghajan and A. Cavallaro, *Multi-camera networks: principles and applications*. Academic press, 2009.
- [11] A. Mavrinac and X. Chen, "Modeling coverage in camera networks: A survey," *International journal of computer vision*, vol. 101, no. 1, pp. 205–226, 2013.
- [12] S. Ó. Murphy, C. Sreenan, and K. N. Brown, "Autonomous unmanned aerial vehicle for search and rescue using software defined radio," in *2019 IEEE 89th Vehicular Technology Conference (VTC2019-Spring)*. IEEE, 2019, pp. 1–6.
- [13] F. Zafari, A. Gkelias, and K. K. Leung, "A survey of indoor localization systems and technologies," *IEEE Communications Surveys & Tutorials*, vol. 21, no. 3, pp. 2568–2599, 2019.
- [14] A. Zanella, "Best practice in rss measurements and ranging," *IEEE Communications Surveys & Tutorials*, vol. 18, no. 4, pp. 2662–2686, 2016.
- [15] S. Lathuilière, B. Massé, P. Mesejo, and R. Horaud, "Neural network based reinforcement learning for audio-visual gaze control in human-robot interaction," *Pattern Recognition Letters*, vol. 118, pp. 61–71, 2019.
- [16] J. Redmon, S. Divvala, R. Girshick, and A. Farhadi, "You only look once: Unified, real-time object detection," in *Proceedings of the IEEE conference on computer vision and pattern recognition*, 2016, pp. 779–788.
- [17] A. Goldsmith, *Wireless Communications*. Cambridge University Press, 2005.
- [18] Y. Zhuang, J. Yang, Y. Li, L. Qi, and N. El-Sheimy, "Smartphone-based indoor localization with bluetooth low energy beacons," *Sensors*, vol. 16, no. 5, p. 596, 2016.
- [19] M. Vollmer and K.-P. Möllmann, "High speed and slow motion: the technology of modern high speed cameras," *Physics Education*, vol. 46, no. 2, p. 191, 2011.
- [20] V. Cantón Paterna, A. Calveras Auge, J. Paradells Aspas, and M. A. Perez Bullones, "A bluetooth low energy indoor positioning system with channel diversity, weighted trilateration and kalman filtering," *Sensors*, vol. 17, no. 12, p. 2927, 2017.